Taylor & Francis
Taylor & Francis Group

RESEARCH PAPER

Check for updates

Adaptation to hypoxia in *Drosophila melanogaster* requires autophagy

Ayelén Valko[a,§], Sebastián Perez-Pandolfo[a,b,§], Eleonora Sorianello[b,c], Andreas Brech[d,e], Pablo Wappner[a,b,f], and Mariana Melani [a,b,f]

[a]Fundación Instituto Leloir, Buenos Aires, Argentina; [b]Consejo Nacional De Investigaciones Científicas Y Técnicas (CONICET), Buenos Aires, Argentina; [c]Laboratorio De Regulación Hipofisaria, Instituto De Medicina Y Biología Experimental (Ibyme-conicet), Buenos Aires, Argentina; [d]Centre for Cancer Cell Reprogramming, Institute of Clinical Medicine, Faculty of Medicine, University of Oslo, Oslo, Norway; [e]Department of Molecular Cell Biology, Institute for Cancer Research, Oslo University Hospital, Oslo, Norway; [f]Departamento De Fisiología, Biología Molecular Y Celular, Facultad De Ciencias Exactas Y Naturales, Universidad De Buenos Aires, Buenos Aires, Argentina

ABSTRACT

Macroautophagy/autophagy, a mechanism of degradation of intracellular material required to sustain cellular homeostasis, is exacerbated under stress conditions like nutrient deprivation, protein aggregation, organelle senescence, pathogen invasion, and hypoxia, among others. Detailed *in vivo* description of autophagic responses triggered by hypoxia is limited. We have characterized the autophagic response induced by hypoxia in *Drosophila melanogaster*. We found that this process is essential for *Drosophila* adaptation and survival because larvae with impaired autophagy are hypersensitive to low oxygen levels. Hypoxia triggers a bona fide autophagic response, as evaluated by several autophagy markers including Atg8, LysoTracker, Lamp1, Pi3K59F/Vps34 activity, transcriptional induction of *Atg* genes, as well as by transmission electron microscopy. Autophagy occurs in waves of autophagosome formation and maturation as hypoxia exposure is prolonged. Hypoxia-triggered autophagy is induced cell autonomously, and different tissues are sensitive to hypoxic treatments. We found that hypoxia-induced autophagy depends on the basic autophagy machinery but not on the hypoxia master regulator sima/HIF1A. Overall, our studies lay the foundation for using *D. melanogaster* as a model system for studying autophagy under hypoxic conditions, which, in combination with the potency of genetic manipulations available in this organism, provides a platform for studying the involvement of autophagy in hypoxia-associated pathologies and developmentally regulated processes.

Abbreviations: Atg: autophagy-related; FYVE: zinc finger domain from Fab1 (yeast ortholog of PIKfyve); GFP: green fluorescent protein; HIF: hypoxia-inducible factor; *hsf: heat shock factor*; Hx: hypoxia; mCh: mCherry; PtdIns: phosphatidylinositol; PtdIns3P: phosphatidylinositol-3-phosphate; Rheb: Ras homolog enriched in brain; sima: similar; Stv: Starvation; TEM: transmission electron microscopy; Tor: target of rapamycin; UAS: upstream activating sequence; Vps: vacuolar protein sorting.

Introduction

Macroautophagy/autophagy is an evolutionarily conserved, catabolic process that can degrade soluble or aggregated proteins, organelles, and cellular pathogens like bacteria and viruses. In the past decades, autophagy has been described as a key mechanism in animal development [1,2]. At fertilization, sperm mitochondria are eliminated from the ooplasm by autophagy, a process that has been described both in *Caenorhabditis elegans* and mice zygotes [3,4]. Furthermore, autophagic activity has been detected during the first mitotic divisions after fertilization, a period at which zygotically encoded proteins are synthesized [5]. In mice, autophagy is believed to function as a central source of amino acids for protein synthesis at pre-implantation stages. After birth, autophagy is activated again to cope with newborn's energetic demands until mother's milk becomes available [6]. In fly development, autophagy plays critical roles during embryogenesis [7], and

also in post embryogenic developmentally regulated processes, such as those taking place in metamorphosis. Particularly, the larval intestine, salivary glands, and the fat body are degraded by autophagy during this critical period, and impairment of autophagy results in organismal death [8–11].

Beyond its function in development, autophagy has been studied mostly as an adaptive response to various stressful conditions such as nutrient deprivation, protein aggregation, and pathogen invasion, to mention a few [12]. Hypoxia is certainly a stressful condition for cells, mainly because mitochondrial oxidative phosphorylation is halted, energy production is severely compromised, and generation of mitochondrial reactive oxygen species is enhanced [13,14]. Thus, hypoxia can be a deleterious insult associated with pathologies such as stroke and ischemic cardiovascular disease [15]. Hypoxia-induced autophagy has been demonstrated in various model systems, including mammalian cultured cells,

plants, and worms [16–20], and in some of these studies, it has been shown that autophagy has a direct impact on the prolongation of life span under low O_2 concentrations [20]. However, whether or not adaptation to hypoxia requires autophagy has not been investigated in depth in *Drosophila*, although there are some conflicting reports about this [21–23].

We have set out to investigate the occurrence of an autophagic response to hypoxia in *Drosophila* and found that hypoxia induces a bona fide autophagic response, as revealed by the analysis of several autophagy markers. This response, which shares most features with starvation-induced autophagy, is independent of the HIF1A/HIFα homolog sima and is vital for adaptation of the larvae to low oxygen levels. Tissue-specific analysis of Atg8 nucleation revealed that each tissue has a specific threshold for triggering autophagy, and that basal levels of autophagy vary greatly among different organs. Interestingly, all tissues analyzed can fine-tune the autophagic response proportionally to the intensity or duration of the hypoxic insult. *Drosophila* can provide an excellent model system to study the genetic regulation of autophagy-dependent adaptation of cells and organs to low oxygen availability in physiological and pathological contexts.

Results

Autophagy is required for adaptation of Drosophila *larvae to low O_2 levels*

We began by comparing the susceptibility to hypoxia of wild type vs. autophagy mutant larvae. In normoxia (21% O_2), autophagy mutants typically progress through embryogenesis and larval development normally, with lethality manifesting at wandering larval or pupal stages [24–28]. To evaluate sensitivity to hypoxia of autophagy mutants, we exposed control or mutant first-instar larvae to either normoxia or hypoxia (4% O_2), for a period of 56 h, after which we counted the number of living larvae. Whereas viability of control larvae was not significantly different in normoxia vs. hypoxia (Figure 1), autophagy mutant larvae showed significant survival reduction in hypoxia, suggesting that autophagy is an essential adaptive response to low oxygen conditions. As previously reported, *sima*[KG07607] mutant larvae did not survive to the hypoxic treatment (Figure 1) [29].

Hypoxia triggers a bona fide autophagic response

As a first approach to evaluate autophagy under hypoxic conditions, we analyzed the behavior of the autophagy marker mCh-Atg8. We compared the extent of Atg8 nucleation in fat body cells of well-fed third-instar larvae with that of larvae subjected to 6 h starvation, as well as that in cells of well-fed third-instar larvae exposed to 4% O_2 for 6 h. mCh-Atg8 was ubiquitously distributed throughout the cell under normoxic well-fed conditions [25], while after 6 h of hypoxia, Atg8 *foci* could be clearly detected, and the extent of nucleation was comparable to that of larvae subjected to 6 h starvation (Figure 2A). We also evaluated autophagy activation by analyzing the lysosomal markers LysoTracker and GFP-Lamp1
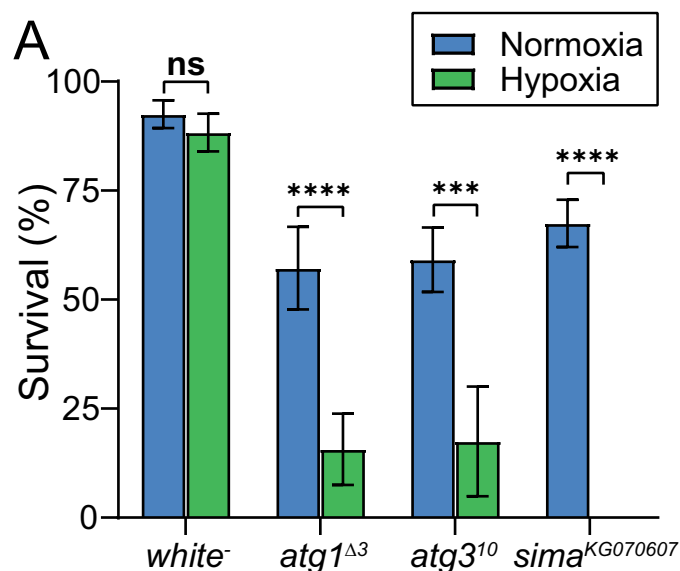

Figure 1. Autophagy is required for survival in hypoxia. Quantification of the larvae that survived after 56 h of either normoxic (21% O_2, blue bars) or hypoxic (4% O_2, green bars) conditions expressed as percentage (%). Control (*white*[1118]), autophagy mutants (*atg1*[Δ3D] and *atg3*[10]), and *sima*[KG07607] are compared. Larvae of the control genotype (*white*[1118]) show no significant sensitivity to hypoxia, whereas both *atg1*[Δ3D] and *atg3*[10] mutants show a significant decrease of survival under hypoxia. All *sima*[KG07607] mutant larvae die under hypoxia. Survival percentage was calculated in at least three independent experiments. Statistical analysis was performed by two-tailed, unpaired Student's *t*-test. N = 7–10 (7–10 plates with 20 larvae in each plate).

[25,30] and found that lysosomes accumulated both under hypoxia and starvation conditions (Figure 2B,C). These results strengthen the notion that hypoxia induces autophagy in *Drosophila* larval fat body cells *in vivo*.

Pi3K59F/Vps34 catalyzes the conversion of phosphatidyl-inositol (PtdIns) to PtdIns3P. Under basal conditions, this phosphorylation takes place mainly in membranes of early endosomes [28], while under autophagic conditions Pi3K59F/Vps34 translocates to specific subdomains of the endoplasmic reticulum as a component of the nucleation complex, and PtdIns3P is deposited at these sites, triggering the formation of omegasomes, the earliest autophagic structures identified, from where phagophores emerge [28,31,32]. We used a reporter of Pi3K59F/Vps34 activity (GFP-2xFYVE) to analyze autophagic activation of Pi3K59F/Vps34 under hypoxic conditions and found that hypoxia resulted in activation of this kinase, as reported by an increase in the number of GFP-2xFYVE *foci* at the cell periphery (Figure 2D) [32]. These data suggest that hypoxia triggers autophagic activation of Pi3K59F/Vps34, supporting again the notion that a bona fide autophagic response is activated under these conditions.

Next, we used quantitative real-time PCR to determine if the autophagic response triggered by hypoxia includes transcriptional activation of *atg* genes. We found that *atg5, atg8a,* and *atg6* mRNA levels were higher in hypoxia- than in normoxia-grown larvae, and that the extent of induction of these transcripts was comparable to that triggered by starvation (Figure 2E). The *hsf* mRNA, a well-characterized hypoxia-inducible gene, was used as a positive control of the hypoxic treatment. Finally, we analyzed fat body cells by TEM, using the number of autophagosomes as readout. We detected
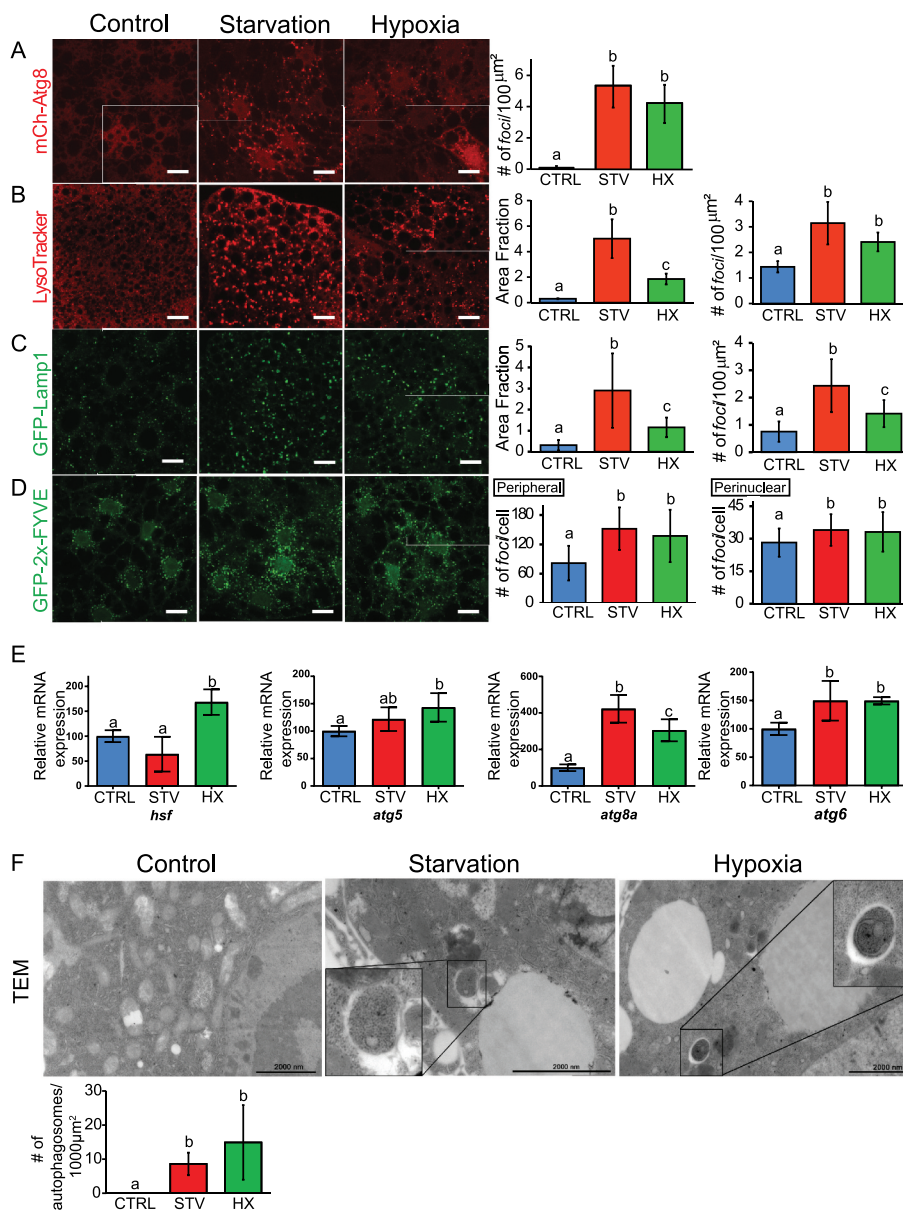
Figure 2. Hypoxia induces a genuine autophagic response. (A–D) Confocal images of fat body cells of third-instar larvae expressing mCherry-Atg8 (A), GFP-Lamp1 (C), or GFP-2xFYVE (D) under control of an act-Gal4 driver, or wild-type larvae stained with LysoTracker (B). For each genotype, animals were fed at 21% O_2 (CTRL; blue bars), starved at 21% O_2 (STV; red bars), or fed at 4% O_2 (HX; green bars). (A) mCherry-Atg8 is distributed homogenously throughout the cells in control larvae, and nucleated in *foci* after 6 h of starvation or hypoxia, indicating the formation of autophagosomes. The bar graph shows the number of mCh-Atg8 *foci* per 100 μm² ($N = 10$). (B) LysoTracker staining and (C) GFP-Lamp1 signal increase 12 h after starvation or hypoxia exposure. The plots on the right show the area fraction covered by the fluorescent signal and the number of *foci* per area for each of the markers ($N = 15$). (D) GFP-2xFYVE signal reporting PtdIns3P amount and distribution. Perinuclear GFP-2xFYVE stains early endosomes, and *foci* at the cell periphery correspond to autophagosomes. Bar graphs show the number of peripheral or perinuclear *foci* per cell (see Materials and methods); $N = 10$–15 for each condition. One-way ANOVA followed by Tukey's test with a confidence interval higher than 95% ($p < 0.05$). Scale bar: 20 μm. (E) mRNA levels of the indicated genes were measured by qRT-PCR in homogenates from whole third-instar larvae grown under control conditions (CTRL), or subjected to 6 h of starvation (STV) or hypoxia (4% O_2) (HX). Statistical analysis was performed by one-way ANOVA followed by Tukey's test with a confidence interval higher than 95% ($p < 0.05$). (F) Transmission electron microscopy images of fat body cells of third-instar larvae grown under control conditions or subjected to starvation or hypoxia for 6 h. An autophagosome is zoomed-in for each experimental condition. The graph depicts the number of autophagosomes per area. One-way ANOVA followed by Tukey's test with a confidence interval higher than 95% ($p < 0.05$).

a minimal number of autophagosomes in control tissues, whereas in fat body cells of larvae exposed to hypoxia or subjected to starvation these structures increased significantly (Figure 2F). These observations confirm that autophagy is induced by hypoxia in *Drosophila* larvae.

To rule out that activation of autophagy under hypoxia is due to starvation derived from a potential failure of the larvae to feed in low oxygen conditions, we performed a feeding behavior assay. We cultured third-instar larvae in blue-colored medium under normoxia or hypoxia for different time periods and analyzed intestine coloring as previously reported [23]. At all time points analyzed, we found comparable staining of the intestine in normoxia- vs. hypoxia-grown larvae, implying that hypoxia did not provoke starvation in this setting (Figure S1). Thus, by utilizing six different strategies, we conclude that hypoxia triggers a genuine autophagic

response that, overall, is comparable to starvation-induced autophagy.

Progression of autophagy under hypoxia or starvation displays a periodic pattern

To further characterize the autophagic response to hypoxia, we made use of the autophagy flux reporter (GFP-mCh-Atg8) that allows to distinguish non-degradative (autophagosomes) from degradative (autolysosomes) structures, based on the differential pH-sensitivity of the fluorophores GFP and mCherry (Figure 3A,B) [33]. Whereas both GFP and mCherry fluoresce at basic or neutral pH in autophagosomes, GFP fluorescence is inactivated in acidic autolysosomes [30,34,35]. We noticed that activation of autophagy by hypoxia had a longer lag phase than that induced by starvation, as it took 1–2 h longer to become detectable with this reporter (Figure 3C–F). However, once they started, the two autophagic responses followed a similar temporal pattern. Both starvation- and hypoxia-
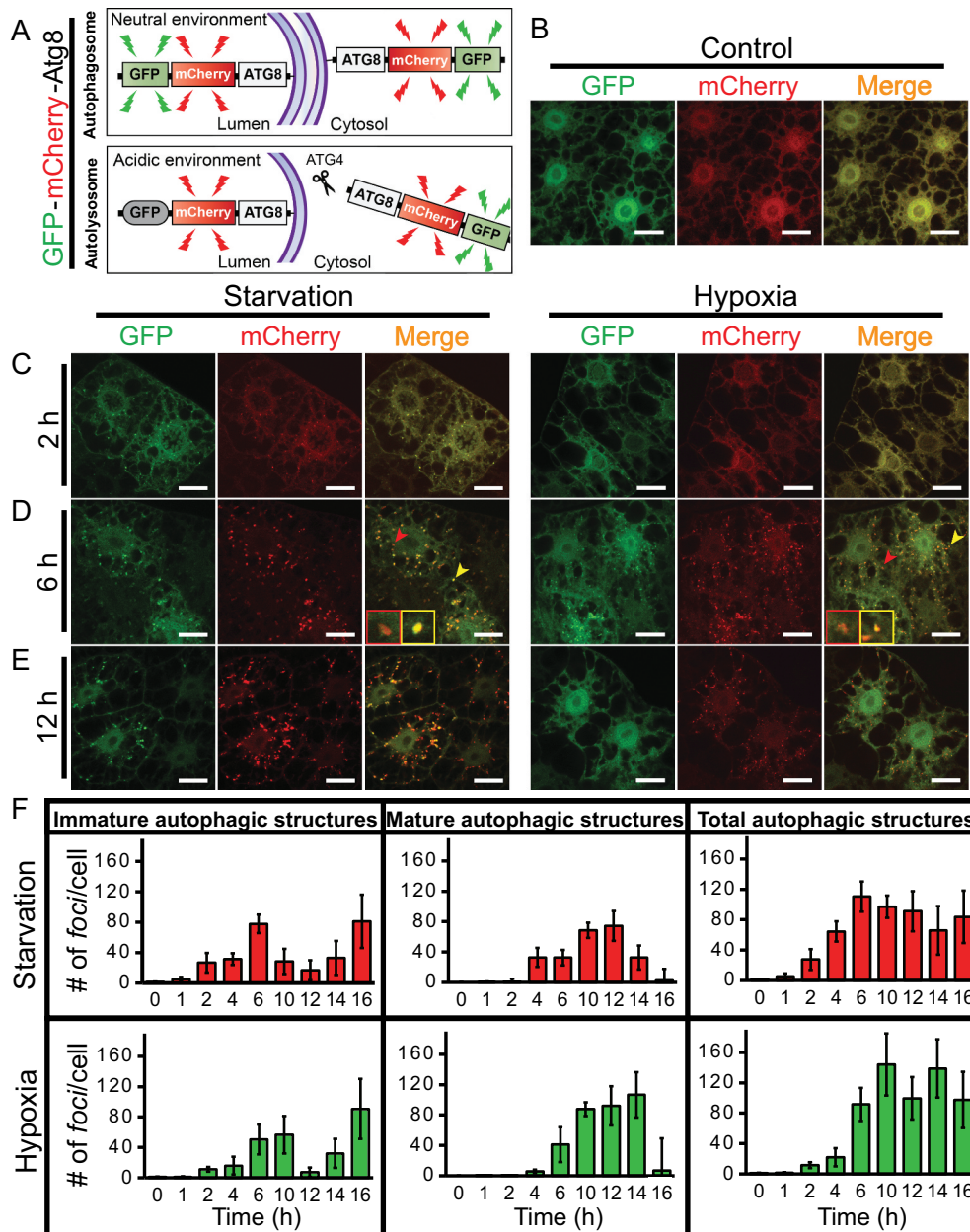

Figure 3. Hypoxia- and starvation-induced autophagy follow similar progression profiles. (A) Schematic representation of the behavior of the GFP-mCherry-Atg8 reporter in response to changes of pH. At basic or neutral pH (top panel), both mCherry and GFP fluoresce; while at acidic pH, GFP does not fluoresce and only the mCherry signal outlasts (e.g., in autolysosomes). (B–E) Confocal images of fat body cells of third-instar larvae expressing GFP-mCherry-Atg8 driven by *act*-Gal4. (B) Control well-fed animals grown at 21% O_2: GFP-mCherry-Atg8 is distributed homogenously in the cells. (C) After 2 h of starvation or hypoxia (4% O_2) a few GFP+ mCherry+ *puncta* are detected (autophagosomes); (D) After 6 h of either treatment, a mixed population of autophagosomes (GFP+ mCherry+, yellow arrowhead) and autolysosomes (GFP− mCherry+, red arrowhead) is observed. The insets show magnified images of an autophagosome and an autolysosome, respectively. (E) At 12 h of treatment, the population of autophagic structures is composed mainly of autolysosomes. (F) Bar graphs show quantification of the number of immature autophagic structures (green + red *foci*), mature autophagic structures (red *foci*) and total autophagic structures at the indicated time points; $N = 10$ for each time point. Scale bar: 20 μm.

induced autophagy took place with a similar periodic pattern, displaying a period of 10–12 h (Figure 3F). Periodic oscillations could be detected in the number of both autophagosomes and autolysosomes, although oscillations of the former and the latter were out of phase (Figure 3F). The total number of autophagic structures remained constant after reaching a maximum at 6 h for starvation-induced autophagy, and at 10 h for hypoxic autophagy. Taken together, this set of results indicates that the autophagic flux in *Drosophila* larvae is not constant, but rather, there are waves of biogenesis and maturation of autophagosomes, and that hypoxia- and starvation-induced autophagy display comparable patterns of progression.

Hypoxia-induced autophagy requires canonical autophagy genes but not the hypoxia-inducible factor sima

We set out to characterize the genetic requirements of this response. In mammalian cultured cells, it has been reported that the requirement of ULK1 or ULK2 for autophagy depends on the autophagic stimulus [36]. In *Drosophila*, Atg1 initiates starvation-induced autophagy [25,32], although alternative signals can induce autophagy independently of this kinase [37]. Along the same line, several publications have shown the existence of autophagic responses that are independent of the Pi3K59F/Vps34 nucleation complex [38,39] or other components of the autophagy cascade [40]. To evaluate the genetic requirements of hypoxia-induced autophagy, we expressed different double-stranded RNAs against autophagy genes in random groups of larval cells *in vivo*, by utilizing the "flip-out" technique [41], and assessed the extent of mCh-Atg8 nucleation in the fat body. As depicted in Figure 4A–G, hypoxia-dependent autophagy was not induced in *atg1, atg17, pi3k59f/vps34, atg6, atg5*, or *atg7* loss-of-function clones, and we found no evidence of apoptosis being activated neither in the clones nor in the surrounding wild-type tissue (Figure S2). Similarly to starvation-induced autophagy [25], overactivation of the Tor pathway by Rheb overexpression prevented induction of hypoxia-triggered autophagy (Figure 4H).

Next, we investigated if the HIF1A subunit homolog sima is required for hypoxia-induced autophagy. We analyzed mCh-Atg8 nucleation in fat body cells that expressed a previously characterized RNAi against *sima*, by using the flip-out technique [42,43]. We found that hypoxia-induced Atg8 nucleation was not affected in *sima* knockdown cells compared to neighboring control cells (Figure 5A), indicating that Sima is not required for autophagy induction under hypoxia. We also analyzed LysoTracker incorporation in fat body cells of *sima*^{KG07607} homozygous mutants vs. control larvae. Consistent with the above RNAi-based observations, in *sima* mutant larvae, hypoxia-induced autophagy was normally triggered, indicating that Sima was dispensable for
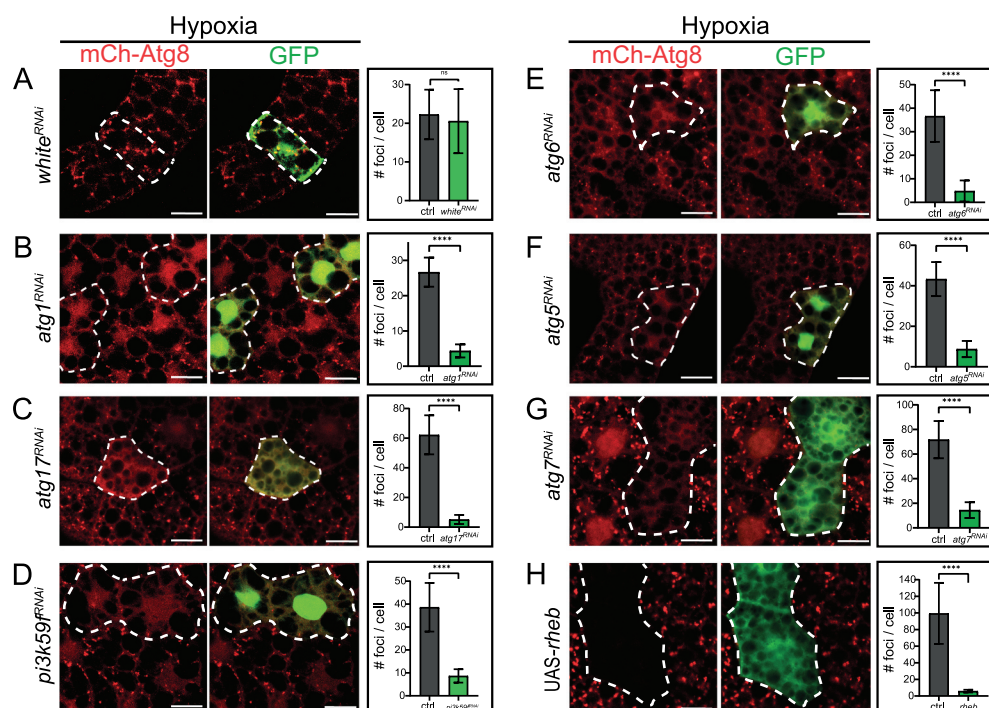

Figure 4. Hypoxia-induced autophagy requires classical autophagy genes. Confocal images of fat body cells of third-instar larvae exposed to hypoxia (4% O$_2$) for 6 h. mCh-Atg8 was expressed under control of the fat body driver *r4*-Gal4. The indicated UAS-constructs were expressed in random cell clones utilizing the *flip-out* technique. The expression of GFP marks the cells in which expression of the indicated UAS construct occurred. (A) UAS-*white*^{RNAi}, (B) UAS-*atg1*^{RNAi}, (C) UAS-*atg17*^{RNAi}, (D) UAS-*pi3k59f/vps34*^{RNAi}, (E) UAS-*atg6*^{RNAi}, (F) UAS-*atg5*^{RNAi}, (G) UAS-*atg7*^{RNAi}, and (H) UAS-*Rheb*. The bar graphs depict the number of Atg8 *foci* per cell in control cells (gray bars) and flip-out-induced cells (green bars) (*N* = 5–12). Statistical analysis was performed by two-tailed, unpaired Student's *t*-test. Scale bar: 20 μm.
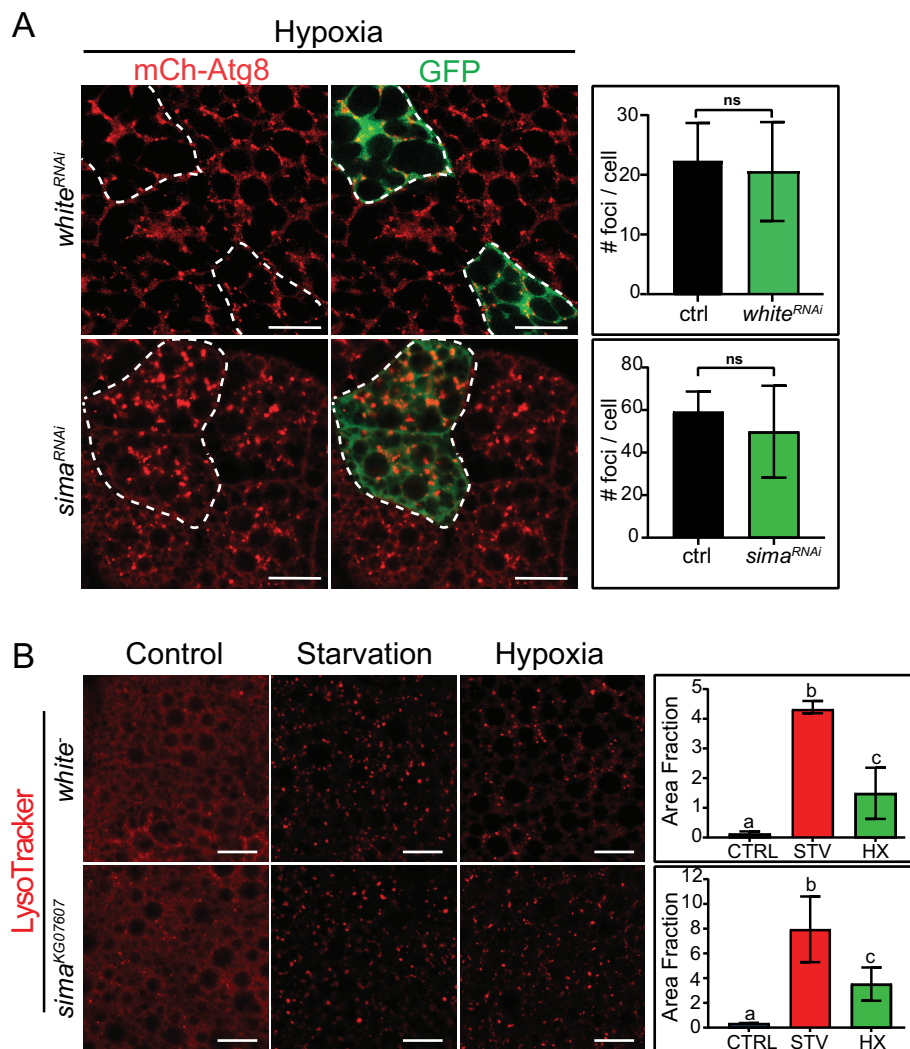
Figure 5. Hypoxia-induced autophagy does not require the HIFα homolog Sima. (A) Confocal image of fat body cells of third-instar larvae subjected to hypoxia (4% O_2) for 6 h. mCh-Atg8 was expressed under control of the fat body driver *r4*-Gal4. *sima^{RNAi}* or *white^{RNAi}* were expressed in random cell clones with the *flip-out* technique. The expression of GFP marks the cells in which expression of the double-stranded RNAs occurred. The bar graph depicts the number of Atg8 *foci* per cell in control cells (gray bars) and flip-out-induced cells (green bars) ($N = 5–12$). Statistical analysis was performed by two-tailed, unpaired Student's *t*-test. Scale bar: 20 µm. (B) Confocal images of fat body cells of *white^{1118}* or *sima^{KG07607}* larvae stained with LysoTracker. Individuals were either fed at 21% O_2 (CTRL; blue bars), starved at 21% O_2 (STV; red bars), or fed and exposed to 4% O_2 during 12 h (HX; green bars). In tissues from control animals (*white^{1118}*), a few LysoTracker-positive *foci* are detected in feeding-normoxic conditions, while *foci* are larger and more abundant (reflected in the area fraction, bar graph) in tissues from either starved or hypoxic animals. In *sima^{KG07607}* homozygous mutants, LysoTracker is readily incorporated into fat body cells of starved or hypoxic larvae, indicating that Sima is not required for starvation-induced or hypoxia-induced autophagy. The bar graphs display quantification of the area fraction of LysoTracker-positive *foci* ($N = 3–6$). One-way ANOVA followed by Tukey's test with a confidence interval higher than 95% ($p < 0.05$). Scale bar: 20 µm.

starvation-induced autophagy (Figure 5B). These results suggest that the autophagy and HIF pathways act in parallel in the adaptation of *Drosophila* larvae to hypoxia.

Activation and requirement of hypoxia-dependent autophagy in different tissues

We began by assessing the oxygen threshold and minimal time at which autophagy is activated in different larval tissues. We exposed the larvae to 21%, 12%, 8%, or 4% O_2 for 6 h, or to 4% O_2 for different periods of time (0, 0.5, 1, 3, or 6 h), after which we assessed mCh-Atg8 nucleation in various organs. In all the tissues analyzed, we found that the autophagic response was proportional to the strength and duration of the hypoxic stimulus (Figure 6 and Figure S3). Interestingly, the brain and tracheal cells displayed high levels of basal

autophagic activity, which was enhanced by hypoxia or starvation (Figure 6 and Figure S3). To rule out the occurrence of potential autophagy-independent nucleation of Atg8, and to evaluate cell autonomy of hypoxia-triggered autophagy in these organs, we induced *atg17^{RNAi}* knockdown clones with the flip-out technique. We found that in all cases hypoxia- and starvation-induced Atg8 nucleation was impaired by *atg17* knockdown (Figure 7), indicating that Atg8 nucleation reflects a genuine autophagic response, and that autophagy in these organs is induced in a cell-autonomous manner in response to starvation or hypoxia.

Having stablished that several larval tissues are capable of triggering autophagy in response to hypoxia, we wondered if this response is necessary in the different tissues for adaptation of the whole organism to hypoxia. We utilized different tissue-specific Gal4 drivers to express *atg17^{RNAi}* to inhibit
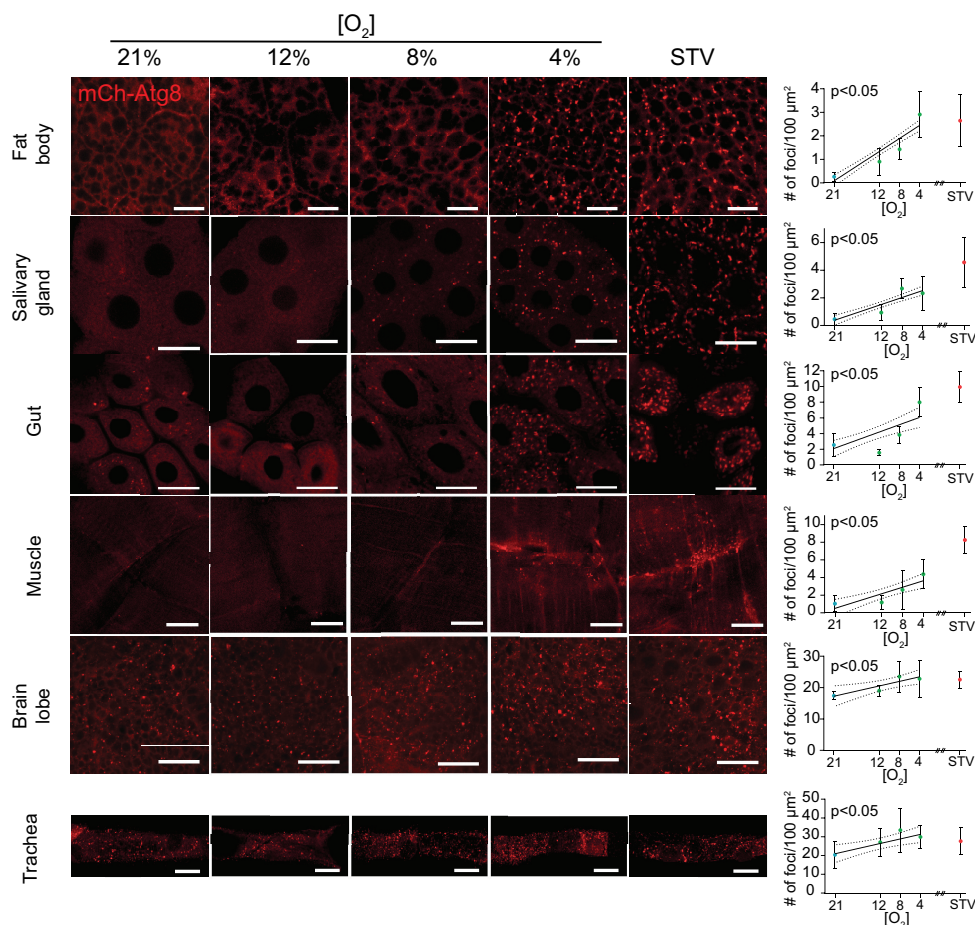
Figure 6. Tissue sensitivity to decreasing oxygen concentrations. Confocal images of the indicated tissues dissected from third-instar larvae exposed for 6 h to the indicated O_2 concentrations, or starved for 6 h. mCh-Atg8 was expressed under control of its own promoter. Graphs depict a linear regression of the number of Atg8 *foci* per 100 μm^2. The autophagic response is proportional to the strength of the hypoxic stimulus. The brain and tracheal cells display high basal autophagic activity, which is enhanced by hypoxia. N = 6–30. Scale bar: 20 μm.

autophagy and assessed larval viability after 56 h of hypoxic treatment. While expression of *atg17^RNAi* with a control adult-specific Gal4 driver (*rhodopsin*-Gal4) did not compromise larval viability in hypoxia (Figure 8A), ubiquitous expression of the same RNAi in larvae resulted in lethality under hypoxic conditions (Figure 8B), with the effect being similar to that observed in mutants that affect autophagy genes (Figure 1). Likewise, restricted expression of *atg17^RNAi* in specific larval tissues, including fat body, salivary glands, muscles, brain, or tracheae, compromised larval survival significantly (Figure 8C–G), indicating that adaptation to hypoxia requires autophagy induction in all these tissues. This set of results suggests that the autophagic response to hypoxia is essential in every tissue for adaptation of the larva to low oxygen conditions.

Discussion

We have performed a characterization of the autophagic response to hypoxia in *Drosophila*, a model system in which this response had not been studied in depth [21–23]. We found that mechanistically hypoxic autophagy is executed by the same machinery as starvation-triggered autophagy as all the autophagy genes that we have tested are equally needed in both conditions. All the different autophagy readouts that we have evaluated, including autophagosome and autophagy flux fluorescent reporters, lysosomal probes, and the Pi3K59F/ Vps34 activity reporter, were similarly induced under hypoxic or starvation conditions. Moreover, we found similar transcriptional activation of some *atg* genes in response to both stimuli, and finally, by transmission electron microscopy we confirmed that hypoxia triggers a bona fide autophagic response in *Drosophila* larvae.

Interestingly, we found that autophagosome formation and maturation under both starvation- and hypoxia-induced autophagy follow a temporal oscillatory pattern in which the maximal number of autophagosomes and autolysosomes are out of phase, resulting in a fairly similar number of total autophagic structures after 6–10 h of stimulus. Even though autophagy has been shown to display a circadian pattern in other biological settings [44–46], in this case, since the larvae were not grown under controlled dark-light conditions, the
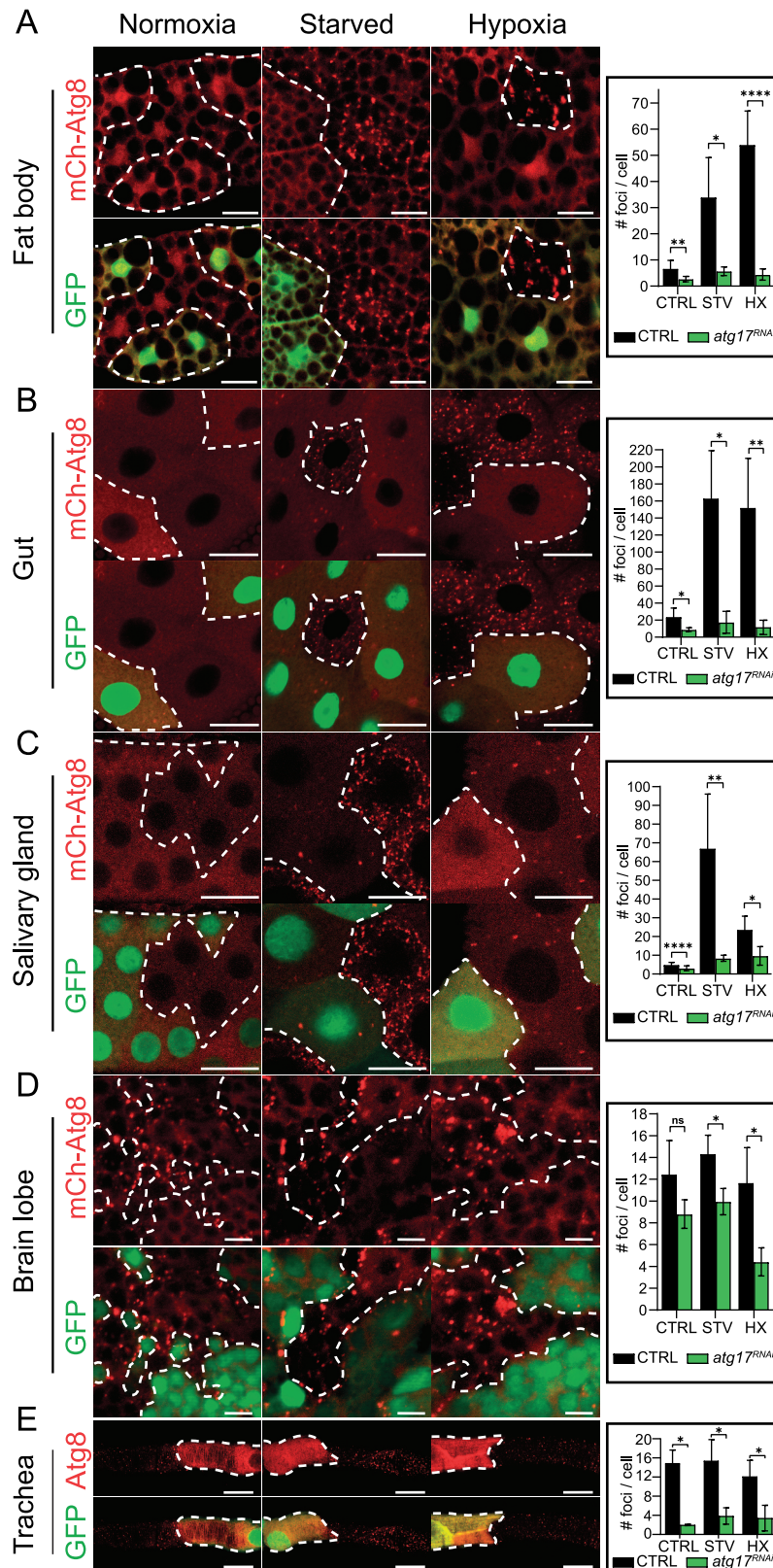
Figure 7. Hypoxia-induced autophagy is cell-autonomous. Confocal images of different tissues dissected from third-instar larvae grown under the indicated condition [(A) fat body; (B) gut; (C) intestine; (D) salivary gland; (F) brain lobe; and (G) tracheae]. mCh-Atg8 was expressed under control of its own promoter. UAS-*atg17^RNAi* was expressed in random cell clones utilizing the *flip-out* technique. The expression of GFP marks the cells in which expression of the corresponding UAS construct occurred. The number of Atg8 foci in control and *atg17^RNAi* cells was quantified (*N* = 2–15). Note that the formation of mCh-Atg8 *foci* is abrogated in *atg17* knockdown clones. Statistical analysis was performed by two-tailed, unpaired Student's *t*-test. Scale bar (A, B, C, E): 20 µm; (D): 5 µm.
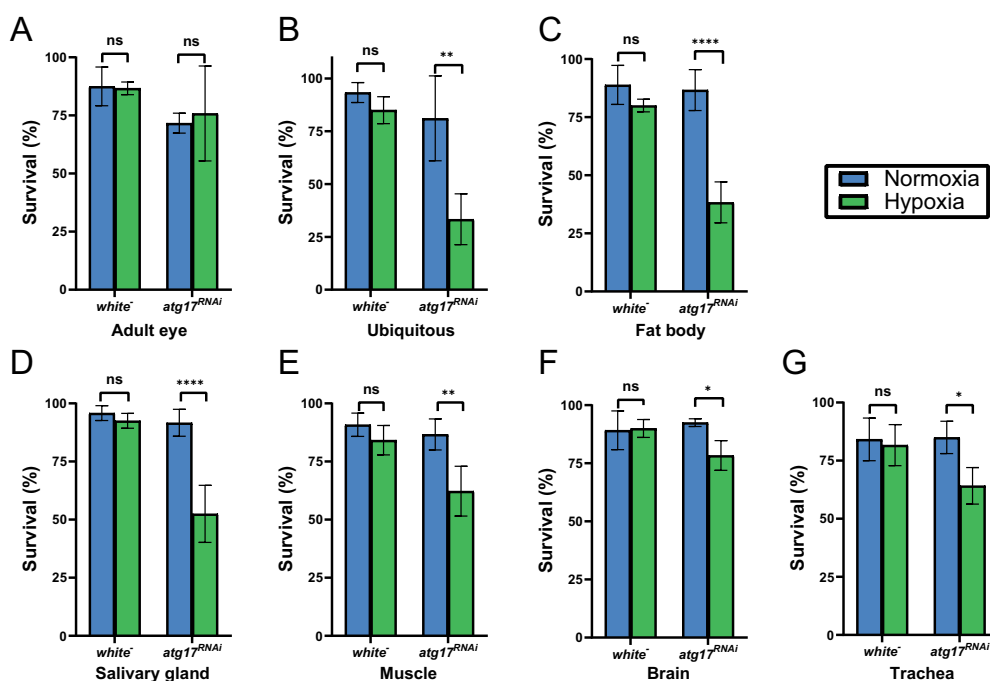
Figure 8. Hypoxia-induced autophagy is required in several tissues for larval viability. Quantification of the larvae that survived after 56 h either in normoxia (21% O_2, blue bars) or hypoxia (4% O_2, green bars), expressed as percentage. Thirty first-instar larvae of the *white*^{1118} control genotype or expressing *atg17*^{RNAi} with different Gal4 drivers [(A) adult eye: *rh5*-Gal4; (B) ubiquitous: *da*-Gal4; (C) fat body: *ppl*-Gal4; (D) salivary glands: *fkh*-Gal4; (E) muscle: *dmef2*-Gal4; (F) pan-neuronal: *elav*-Gal4; and (G) tracheae: *btl*-Gal4) were sorted into fresh vials and let to developed for 56 h either in normoxia or at 4% O_2. Survival percentage was assessed in at least two independent experiments. Autophagy is required in all the tested organs for larval survival. Statistical analysis was performed by two-tailed, unpaired Student's *t*-test. $N = 3–6$ (3–6 plates with 30 larvae for each plate).

periodicity of autophagosome formation/maturation might rather reflect periodic exhaustion and reposition cycles of components of the autophagy machinery.

We found that autophagy is required for adaptation of *Drosophila* larvae to low oxygen conditions, and that the Tor pathway is a critical regulator of its induction. How does the Tor pathway convey the hypoxic stimulus to trigger autophagy? Studies carried out both in mammalian cells and *Drosophila* have revealed that MTOR/Tor activity is hindered by hypoxia through a mechanism that involves HIF-dependent activation of DDIT4/REDD1, or of its *Drosophila* orthologs scyl (scylla) and chrb (charybde), which in turn potentiate the activity of the Tor inhibitor Tsc1-gig/Tsc2 [47,48]. However, HIF-independent regulation of MTOR/Tor and its targets has also been reported [23,49], so in principle, depending on the biological setting, HIF-dependent and HIF-independent mechanisms seem to contribute to MTOR/Tor inhibition in hypoxia. Our data support that the latter mechanism prevails in developing *Drosophila* larvae as activation of the autophagic response to hypoxia takes place normally in sima mutants or sima knockdown cells. In line with these results, global analysis of hypoxia-dependent gene expression in mammalian cells has shown that hypoxia can induce the expression of some autophagy genes in a HIF-independent manner [50].

We found that the larval tissues analyzed can accurately tune the autophagic response proportionally to the intensity or duration of the stimulus. Interestingly, the brain and tracheae display high levels of basal autophagy that are increased after exposure to hypoxia or starvation. High basal levels of autophagy in some specific organs are intriguing, and could be related to tissue-specific energy stores and/or energy demands. Interestingly, it has been reported that the larval ring gland also displays basal autophagy in fully fed larvae and that this tissue can further increase the autophagic response when larvae are starved [51]. Tissue- or organ-specific sensitivity for triggering autophagy has been reported in other model systems as well. For example, in neonatal mice, which physiologically experience a sudden shortage of placental nutrient supplies, it was reported that the heart, diaphragm, and lung cells display an autophagic response that is enhanced, and particularly fast in comparison to other organs, such as the liver or the skeletal muscles [6]. Related with this, we found that autophagy activation is required in each of the tested tissues to sustain viability under low O_2 concentrations. Altogether, these results suggest that autophagy can be modulated in an organ-specific manner to cope with tissue-specific energetic demands essential for organismal adaptation to hypoxia.

Tissue-specific autophagy activation is probably part of an evolutionarily successful strategy to integrate developmental programs with adaptation to stress conditions. Future studies are required to shed light on the molecular basis and physiological significance of tissue-specific

sensitivity to autophagy activation in response to different stressors including hypoxia.

Materials and methods

Fly stocks

Flies were raised at 25°C in standard cornmeal/agar medium (10 g/l agar [VanRossum, MATPRI0153], 20 g/l baking yeast, 66.5 g/l cornmeal, 40 g/l sucrose [Anedra, AN00711809], 4.5 ml/l propionic acid [Cicarelli, 1085110], and 0.18 g/l Nipagin [VanRossum, MATPRI0350]). In all experiments, larvae of the desired genotype were sorted 24 h after egg laying. In most experiments, 30–40 larvae were grown at 25°C from first instar to early third instar in plates with enriched medium containing 3.4% baking yeast and 6% sucrose (Anedra, AN00711809). Then, third-instar larvae were starved on agar plates or exposed to 4% O_2 in colored enriched medium as described below during different periods of time depending on the experiment. The following *Drosophila melanogaster* lines were obtained from the Bloomington Stock Center (http://flystocks.bio.indiana.edu): *yw* (BL 64401), *actin*-Gal4 (BL 4414), *ppl*-Gal4 (BL 58768), *elav*-Gal4 (BL 458), *da*-Gal4 (BL 55851), *dmef2*-Gal4 (BL 27390), *fkh*-Gal4 (BL 78060), *rh5*-Gal4 (BL7458), UAS-GFP-mCherry-*atg8* (BL 37749), UAS-GFP-2xFYVE (BL 42712), UAS-*white*^{RNAi} (BL 33613), UAS-*vps34*^{RNAi} (BL 33384). UAS-*atg17*^{RNAi} (BL 36918), UAS-*atg7*^{RNAi} (BL 34369), UAS-*atg5*^{RNAi} (BL 27551), UAS-*Rheb* (BL 9688), UAS-*rpr* (BL 5823), or from the Vienna Drosophila Resource Center (https://stockcenter.vdrc.at): UAS-*atg1*^{RNAi} (v16133), and UAS-*atg6*^{RNAi} (v22123). UAS-mCherry-*atg8* and UAS-*vps34*^{DN} were kindly provided by Thomas Neufeld [28] (University of Minnesota, Minneapolis). *btl*-Gal4 was provided by the Hayashi Lab [52] (Riken Center for Biosystems Dynamics Research, Japan), UAS-GFP-*lamp1* was provided by Helmut Kramer [53] (University of Texas Southwestern Medical Center, Dallas). The *atg1*$^{[Δ3D]}$ and *atg3*^{10} mutants were a generous gift from Gábor Juhász (Eotvos Lorand University, Budapest). The *sima*^{KG07607} mutant was previously described [29].

Hypoxic treatment

Larvae of the indicated genotypes were grown from first instar to early third instar in plates with enriched medium containing yeast 3.4% and sucrose 6% at 25°C. Then, 15–20 larvae were transferred to a fresh plate with enriched medium and incubated at 25°C for the indicated time periods either in normoxia (21% O_2) or hypoxia (4% O_2) in a Forma Series II Thermo Scientific incubator by regulating the proportions of nitrogen and oxygen. For survival studies, 20 first-instar larvae of each genotype were placed in plates with enriched medium in normoxia or hypoxia (4% O_2) until they have reached the third instar when the number of surviving larvae was counted.

To assess feeding in hypoxia, third-instar larvae were kept in normoxia or exposed to hypoxia in enriched medium containing bromophenol blue (0.08 mg/ml), and after 2–12 h, the larvae were photographed under an MVX10 Olympus stereoscope.

Staining, visualization, and image processing of Drosophila tissues

Fat bodies from third-instar larvae were dissected in phosphate-buffered saline (PBS; 8 g/l NaCl, 0.2 g/l KCl, 1.44 g/l Na_2HPO_4, 0.24 g/l KH_2PO_4, pH 7.4) and fixed in 4% methanol-free formaldehyde (Polysciences, 18814-10) for 2 h at room temperature. Afterward, samples were washed three times in PBS-0.1% Triton X-100 (Sigma, T-6878) and mounted in 40% glycerol for direct visualization. When needed, 300 nM 4′,6-diamidine-2-phenylindole (DAPI; Molecular Probes, D1306) was added at the first washing step. For LysoTracker (Invitrogen, L7528) staining, the reagent was added to unfixed tissues and directly visualized as previously described [25]. Tissues were imaged using a Carl Zeiss LSM 710 confocal microscope with a Plan-Neofluor 40×/1.3 NA objective or Plan-Apochromat 63×/1.4 NA oil objective, or a Carl Zeiss LSM 880 confocal microscope with a Plan-Apochromat 20×/0.8 NA objective or Plan-Apochromat 63×/1.4 NA oil objective. LysoTracker signal as well as GFP-Lamp1 fluorescence were quantified by assessing the area fraction with the ImageJ software. For counting GFP-2xFYVE autophagic *foci*, the images were processed as previously described [32]. Briefly, we set a threshold using ImageJ to eliminate the background signal, and then, we divided each cell into a perinuclear and a peripheral region, to count *foci* therein.

Transmission electron microscopy

For TEM sample preparation, larvae were dissected and fixed overnight at 4°C using 2.5% glutaraldehyde in 0.1 M phosphate buffer, pH 7.4, followed by post-fixation in 1% osmium tetroxide for 1 h. Tissues were stained overnight at 4°C in 2% uranyl acetate and dehydrated with ethanol. Samples were then embedded in Epoxy resin (Durcupan, 44611) and 60- to 70-nm sections were cut. Images were obtained using a transmission electron microscope (JEOL-JEM 1230) at 80 kV, and using a Morada digital camera (Olympus Soft Imaging). A total of 15–30 images at 20.000× magnification were obtained from random areas of the sample from at least two animals per genotype. Autophagosomes were identified by their typical morphology characterized by internalized cytosol limited by a double membrane, which often appears to be dilated leaving an electron-lucent lumen visible. The number of autophagosomes was counted and computed per unit area at the fat body.

RNA extraction and cDNA synthesis

Total RNA was isolated from seven third-instar larvae, using 500 μl of Quick-Zol reagent (Kalium Technologies, RAO1011933) following the manufacturer's instructions. Genomic DNA was removed from RNA samples using DNase (Ambion, AM2222). The concentration and integrity of the RNA were determined using NanoDrop (Thermo Fisher Scientific) spectrophotometry. RNA (1 μg) was reverse-transcribed using

M-MLV Reverse Transcriptase (Invitrogen, 10338842) using oligo-dT as a primer. Control reactions omitting reverse transcriptase were used to assess the absence of contaminating genomic DNA in the RNA samples. An additional control without RNA was included.

Real-time PCR

Gene expression was analyzed by quantitative PCR in a CFX96 Touch (Bio-Rad) cycler. The reactions were performed using HOT FIREPol EvaGreen qPCR Mix Plus (ROX; Solis BioDyne, 08-24-0000S), 0.40 µM primers, and 3–25 ng of cDNA, in a final volume of 10.4 µl. Cycle conditions were initial denaturation at 95°C for 15 min, and 40 cycles of denaturation at 95°C for 20 s, annealing at 60°C for 1 min, and extension and optical reading stage at 72°C for 30 s, followed by a dissociation curve consisting of ramping the temperature from 65 to 95°C while continuously collecting fluorescence data. Product purity was confirmed by agarose gel electrophoresis. Relative gene expression levels were calculated according to the comparative cycle threshold (CT) method. Normalized target gene expression relative to rpl29 was obtained by calculating the difference in CT values, the relative change in target transcripts being computed as $2-\Delta CT$. The efficiencies of each target and housekeeping gene amplification were measured and shown to be approximately equal. Oligonucleotides were obtained from Macrogen (Seoul, Korea), and their sequences were the following: *atg5*: Fw 5′-GCACGCACGGCATTGATCTACA-3′,Rv 5′-GCCCTGGGATTTGCTGGAAT-3′; *atg6*: Fw 5′-TATGTTGAGGTGCTCGGCGAGA-3′, Rv 5′-TGGTCCACTGCTCCTCCGAGTT-3′; *atg8a*: Fw 5′-GCAAATATCCAGACCGTGTGCC, Rv 5′-AGCCCATGGTAGCCGATGTT; *hsf*: Fw 5′-ACACCGCAGCCTCACATTATGACC-3′, Rv 5′-ATTTCCCTGGAGCAGCAAGTCCTC-3′; *rpl29*: Fw: 5′-GAACAAGAAGGCCCATCGTA-3′, Rv: 5′-AGTAAACAGGCTTTGGCTTGC-3′. Rpl29 was used as housekeeping gene. Specificity and quality of oligonucleotide sequences for *atg5*, *atg6*, *atg8a*, *hsf*, and *rpl29* were checked using Primer Blast Resource of the NCBI (http://www.ncbi.nlm.nih.gov/tools/primer-blast/).

Statistical analysis

Statistical significance was calculated using one-way analysis of variance (ANOVA) followed by Tukey's test with a 95% confidence interval ($p < 0.05$). In cases where comparison between two treatments was needed, two-tailed, unpaired Student's *t*-test was used instead. See the following table for symbol meanings:

Symbol	Meaning
ns	$p > 0.05$
*	$p \leq 0.05$
**	$p \leq 0.01$
***	$p \leq 0.001$
****	$p \leq 0.0001$

The Grubb's test was used to identify outliers ($p < 0.05$). Normality was tested with the KS test and D'Agostino–Pearson test. To achieve homoscedasticity (Bartlett's test), data were transformed using the functions: log ($n + 1$) in Figure 2A, $n^{\wedge}$ (1/2) in Figure 2B, log $n + 1$ in Figure 2C, and log n for peripheral *foci* in Figure 2D. In most experiments, statistical analyses were executed using GraphPad Prism version 8.01, except in Figure 2A,E where Rstudio version 3.3.1 was employed instead. In these figures, data were transformed to log($n + 1$) (Figure 2A) and log($n + 1$)+1 (Figure 2E), and variances were modeled with the VarIdent function, using the smaller AIC criteria. In all plots, data were represented as mean ± SD. Each experiment was independently repeated at least twice.

ORCID

Mariana Melani http://orcid.org/0000-0002-9491-932X

References

[1] Schneider JL, Cuervo AM. Autophagy and human disease: emerging themes. Curr Opin Genet Dev. 2014;26:16–23.
[2] Mizushima N, Komatsu M. Autophagy: renovation of cells and tissues. Cell. 2011;147(4):728–741.
[3] Al Rawi S, Louvet-Vallée S, Djeddi A, et al. Postfertilization autophagy of sperm organelles prevents paternal mitochondrial DNA transmission. Science. 2011;334(6059):1144–1147.
[4] Sato M, Sato K. Degradation of paternal mitochondria by fertilization-triggered autophagy in C. elegans embryos. Science. 2011;334(6059):1141–1144.
[5] Tsukamoto S, Kuma A, Murakami M, et al. Autophagy is essential for preimplantation development of mouse embryos. Science. 2008;321(5885):117–120.
[6] Kuma A, Hatano M, Matsui M, et al. The role of autophagy during the early neonatal starvation period. Nature. 2004;432 (7020):1032–1036.
[7] Cormier O, Mohseni N, Voytyuk I, et al. Autophagy can promote but is not required for epithelial cell extrusion in the amnioserosa of the Drosophila embryo. Autophagy. 2012;8(2):252–264.
[8] Lee CY, Baehrecke EH. Steroid regulation of autophagic programmed cell death during development. Development. 2001;128(8):1443–1455.
[9] Denton D, Shravage B, Simin R, et al. Autophagy, not apoptosis, is essential for midgut cell death in Drosophila. Curr Biol. 2009;19 (20):1741–1746.

[10] Berry DL, Baehrecke EH. Growth arrest and autophagy are required for salivary gland cell degradation in Drosophila. Cell. 2007;131(6):1137–1148.

[11] Rusten TE, Lindmo K, Juhász G, et al. Programmed autophagy in the Drosophila fat body is induced by ecdysone through regulation of the PI3K pathway. Dev Cell. 2004;7(2):179–192.

[12] Klionsky DJ. Guidelines for the use and interpretation of assays for monitoring autophagy (3rd edition). Autophagy. 2016;12 (1):1–222.

[13] Sokolova IM, Sokolov EP, Haider F. Mitochondrial mechanisms underlying tolerance to fluctuating oxygen conditions: lessons from hypoxia-tolerant organisms. Integr Comp Biol. 2019;59 (4):938–952.

[14] Corrado C, Fontana S. Hypoxia and HIF signaling: one axis with divergent effects. Int J Mol Sci. 2020;21(16):5611.

[15] Semenza GL. Oxygen sensing, homeostasis, and disease. N Engl J Med. 2011;365(6):537–547.

[16] Zhang H, Bosch-Marce M, Shimoda LA, et al. Mitochondrial autophagy is an HIF-1-dependent adaptive metabolic response to hypoxia. J Biol Chem. 2008;283(16):10892–10903.

[17] Bellot G, Garcia-Medina R, Gounon P, et al. Hypoxia-induced autophagy is mediated through hypoxia-inducible factor induction of BNIP3 and BNIP3L via their BH3 domains. Mol Cell Biol. 2009;29 (10):2570–2581.

[18] Wen X, Klionsky DJ. An overview of macroautophagy in yeast. J Mol Biol. 2016;428(9 Pt A):1681–1699.

[19] Chen L, Liao B, Qi H, et al. Autophagy contributes to regulation of the hypoxia response during submergence in Arabidopsis thaliana. Autophagy. 2015;11(12):2233–2246.

[20] Samokhvalov V, Scott BA, Crowder CM. Autophagy protects against hypoxic injury in C. elegans. Autophagy. 2008;4 (8):1034–1041.

[21] Anding AL, Baehrecke EH. Vps15 is required for stress induced and developmentally triggered autophagy and salivary gland protein secretion in Drosophila. Cell Death Differ. 2015;22(3):457–464.

[22] Low P, Varga Á, Pircs K, et al. Impaired proteasomal degradation enhances autophagy via hypoxia signaling in Drosophila. BMC Cell Biol. 2013;14:29.

[23] Lee B, Barretto EC, Grewal SS. TORC1 modulation in adipose tissue is required for organismal adaptation to hypoxia in Drosophila. Nat Commun. 2019;10(1):1878.

[24] Tracy K, Baehrecke EH. The role of autophagy in Drosophila metamorphosis. Curr Top Dev Biol. 2013;103:101–125.

[25] Scott RC, Schuldiner O, Neufeld TP. Role and regulation of starvation-induced autophagy in the Drosophila fat body. Dev Cell. 2004;7(2):167–178.

[26] Shravage BV, Hill JH, Powers CM, et al. Atg6 is required for multiple vesicle trafficking pathways and hematopoiesis in Drosophila. Development. 2013;140(6):1321–1329.

[27] Chang YY, Neufeld TP. An Atg1/Atg13 complex with multiple roles in TOR-mediated autophagy regulation. Mol Biol Cell. 2009;20(7):2004–2014.

[28] Juhasz G, Hill JH, Yan Y, et al. The class III PI(3)K Vps34 promotes autophagy and endocytosis but not TOR signaling in Drosophila. J Cell Biol. 2008;181(4):655–666.

[29] Centanin L, Ratcliffe PJ, Wappner P. Reversion of lethality and growth defects in Fatiga oxygen-sensor mutant flies by loss of hypoxia-inducible factor-alpha/Sima. EMBO Rep. 2005;6 (11):1070–1075.

[30] Lorincz P, Mauvezin C, Juhasz G. Exploring autophagy in Drosophila. Cells. 2017;6(3):22.

[31] Axe EL, Walker SA, Manifava M, et al. Autophagosome formation from membrane compartments enriched in phosphatidylinositol 3-phosphate and dynamically connected to the endoplasmic reticulum. J Cell Biol. 2008;182(4):685–701.

[32] Melani M, Valko A, Romero NM, et al. Zonda is a novel early component of the autophagy pathway in Drosophila. Mol Biol Cell. 2017;28(22):3070–3081.

[33] Mauvezin C, Ayala C, Braden CR, et al. Assays to monitor autophagy in Drosophila. Methods. 2014;68(1):134–139.

[34] Kimura S, Noda T, Yoshimori T. Dissection of the autophagosome maturation process by a novel reporter protein, tandem fluorescent-tagged LC3. Autophagy. 2007;3(5):452–460.

[35] Nezis IP, Shravage BV, Sagona AP, et al. Autophagic degradation of dBruce controls DNA fragmentation in nurse cells during late Drosophila melanogaster oogenesis. J Cell Biol. 2010;190(4):523–531.

[36] Alers S, Löffler AS, Wesselborg S, et al. The incredible ULKs. Cell Commun Signal. 2012;10(1):7.

[37] Braden CR, Neufeld TP. Atg1-independent induction of autophagy by the Drosophila Ulk3 homolog, ADUK. FEBS J. 2016;283 (21):3889–3897.

[38] Codogno P, Mehrpour M, Proikas-Cezanne T. Canonical and non-canonical autophagy: variations on a common theme of self-eating? Nat Rev Mol Cell Biol. 2011;13(1):7–12.

[39] Vicinanza M, Korolchuk V, Ashkenazi A, et al. PI(5)P regulates autophagosome biogenesis. Mol Cell. 2015;57(2):219–234.

[40] Chang TK, Shravage BV, Hayes SD, et al. Uba1 functions in Atg7- and Atg3-independent autophagy. Nat Cell Biol. 2013;15 (9):1067–1078.

[41] Golic KG, Lindquist S. The FLP recombinase of yeast catalyzes site-specific recombination in the Drosophila genome. Cell. 1989;59(3):499–509.

[42] De Lella Ezcurra AL, Bertolin AP, Kim K, et al. miR-190 enhances HIF-dependent responses to hypoxia in drosophila by inhibiting the Prolyl-4-hydroxylase Fatiga. PLoS Genet. 2016;12(5):e1006073.

[43] Bertolin AP, Katz MJ, Yano M, et al. Musashi mediates translational repression of the Drosophila hypoxia inducible factor. Nucleic Acids Res. 2016;44(16):7555–7567.

[44] Czaja MJ, Ding W-X, Donohue TM, et al. Functions of autophagy in normal and diseased liver. Autophagy. 2013;9 (8):1131–1158.

[45] Ma D, Lin JD. Circadian regulation of autophagy rhythm through transcription factor C/EBPbeta. Autophagy. 2012;8(1):124–125.

[46] Wang X, Xu Z, Cai Y, et al. Rheostatic balance of circadian rhythm and autophagy in metabolism and disease. Front Cell Dev Biol. 2020;8:616434.

[47] Brugarolas J, Lei K, Hurley RL, et al. Regulation of mTOR function in response to hypoxia by REDD1 and the TSC1/TSC2 tumor suppressor complex. Genes Dev. 2004;18(23):2893–2904.

[48] Reiling JH, Hafen E. The hypoxia-induced paralogs Scylla and Charybdis inhibit growth by down-regulating S6K activity upstream of TSC in Drosophila. Genes Dev. 2004;18 (23):2879–2892.

[49] Arsham AM, Howell JJ, Simon MC. A novel hypoxia-inducible factor-independent hypoxic response regulating mammalian target of rapamycin and its targets. J Biol Chem. 2003;278 (32):29655–29660.

[50] Perez-Perri JI, Dengler VL, Audetat KA, et al. The TIP60 complex is a conserved coactivator of HIF1A. Cell Rep. 2016;16(1):37–47.

[51] Pan X, Neufeld TP, O'Connor MB. A tissue- and temporal-specific autophagic switch controls drosophila pre-metamorphic nutritional checkpoints. Curr Biol. 2019;29(17):2840–2851 e4.

[52] Ikeya T, Hayashi S. Interplay of Notch and FGF signaling restricts cell fate and MAPK activation in the Drosophila trachea. Development. 1999;126(20):4455–4463.

[53] Pulipparacharuvil S, Akbar MA, Ray S, et al. Drosophila Vps16A is required for trafficking to lysosomes and biogenesis of pigment granules. J Cell Sci. 2005;118(Pt 16):3663–3673.